PNAS
www.pnas.org

Supplementary Information for

Accelerated river avulsion frequency on lowland deltas due to sea-level rise

Austin J. Chadwick[a*], Michael P. Lamb[a], Vamsi Ganti[b,c]

[a]Division of Geological and Planetary Sciences, California Institute of Technology, Pasadena, CA 91125

[b]Department of Geography, University of California, Santa Barbara, CA 93106

[c]Department of Earth Science, University of California, Santa Barbara, CA 93106

* Correspondence may be addressed to Austin J. Chadwick
Email: achadwick@caltech.edu
ORCID: https://orcid.org/0000-0002-2552-0083

This PDF file includes:

Supplementary text
Figures S1 to S2
Tables S1 to S3
SI References

Supplementary text

A. Derivation of numerical model for backwater-scaled avulsions

The numerical model was built on previous work (1) that explored controls on avulsion location on lowland deltas, but did not analyze avulsion frequency and its dependency on relative sea-level rise. The model consisted of a delta with an imposed number of lobes assumed to form a branching pattern, with only one lobe active at a given time (Fig. 1C) (1, 2). Each delta lobe is modeled as a coupled river and floodplain in a quasi-two-dimensional mass balance framework (3, 4),

$$\frac{\partial \eta}{\partial t} + \sigma = -\frac{1}{(1-\lambda_p)}\frac{1}{B}\frac{\partial Q_t}{\partial x} \quad \text{(S1)}$$

where η is channel bed elevation relative to sea level, t is time, σ is relative sea-level rise rate, x is downstream distance, and Q_t is the volumetric sediment transport capacity at position x. Sediment is deposited uniformly over lobe width B with porosity λ_p. At the delta front, fluvial sediment transport transitions to gravity flows and avalanching, and deposition drives foreset progradation. We approximated progradation using a moving-boundary formulation, with a foreset of constant slope S_a set to five times the transport slope (5, 6).

We used the backwater equation to constrain water mass and momentum under quasi-steady flow conditions (3),

$$\frac{dH_w}{dx} = \frac{S - S_f}{1 - Fr^2} + \frac{Fr^2}{1 - Fr^2}\frac{H}{B_w}\frac{dB_w}{dx} \quad \text{(S2)}$$

where H_w is flow depth, S is channel-bed slope, $S_f = C_f Fr^2$ is friction slope, C_f is friction coefficient, Fr is Froude number, and B_w is the width of flow. We assumed flow width was contained by the channel upstream of the river mouth, and expanded at a constant spreading angle offshore (3, 7), here set to 15 degrees. Following recent work (1), the location of the river mouth x_m was set by the intersection of the floodplain profile η_f with sea level ξ_o,

$$x_m = x|_{\eta_f(x) = \xi_o} \quad \text{(S3)}$$

where the floodplain elevation is defined as the sum of the bed elevation and channel depth H_c,

$$\eta_f(x) = \eta(x) + H_c \quad \text{(S4)}$$

Over time, the floodplain in our model aggraded in concert with the channel bed, driving river-mouth advancement. A mobile river mouth was necessary for foreset progradation to drive topset aggradation (1).

We routed sediment in the river according to Engelund-Hansen (8) for total bed-material load,

$$Q_t = B_c\sqrt{RgD^3}\,\frac{\alpha}{C_f}\,(\tau^*)^n \quad \text{(S5)}$$

where R is submerged specific density of sediment, g is gravity, D is the median grain-size of bed material, τ^* is Shields number, and $\alpha = 0.05$ and $n = 2.5$. All sediment delivered to the delta front was captured in the foreset (6, 9).

Following recent work (1), we approximated deltaic evolution using four separate quasi-two-dimensional profiles of predefined width, representing four distinct lobes. At a given time, one delta lobe was active (10, 11) and was governed by Eqs. $(S1 - S5)$. We varied sediment supply at the upstream end with water discharge such that the normal-flow bed slope was held constant, and therefore erosion and deposition were not driven by changes in the ratio of sediment supply to water discharge (12). Inactive lobe shapes were unchanged when abandoned (13) but were partially drowned in cases due to relative sea-level rise.

We used an avulsion criterion given by a critical thickness of aggradation, which we refer to as superelevation ($\Delta\eta$):

$$\Delta\eta(x) \geq H \quad \text{(S6)}$$

in which $H = H^* H_c$ is the aggradation thickness necessary for avulsion, H_c is the bankfull channel depth, and H^* is the avulsion threshold, a dimensionless number that is of order unity (14–16). We triggered an avulsion when and where the floodplain elevation of the active lobe exceeded the floodplain elevation of the lowest-elevation abandoned lobe ($\eta_{f,abandoned}$), evaluated at the same distance downstream from the trunk channel:

$$\Delta\eta(x) = \begin{cases} \eta_f(x) - \eta_{f,abandoned}(x) & \text{for } x \leq x_{m,abandoned} \\ \eta_f(x) - \xi_{sea} & \text{for } x > x_{m,abandoned} \end{cases} \quad \text{(S7)}$$

where $x_{m,abandoned}$ is the stream-wise coordinate of the abandoned-lobe shoreline. Seaward of the abandoned lobe, superelevation is measured relative to sea level (ξ_{sea}) (1, 17). Extreme floods may also affect the timing of any one avulsion (15, 18), but these factors were neglected following previous work (1, 19, 20). For simplicity we ignored the river reach laterally spanning lobes, because lobes are much longer than they are wide (21, 22).

After avulsion, the river was rerouted to the lowest abandoned lobe by joining the bed profile of the active channel upstream of the avulsion site with the bed profile of the new flow path downstream,

$$\eta_{new}(x) = \begin{cases} \mathrm{MIN}\left(\eta_{abandoned1}(x), \eta_{abandoned2}(x), \eta_{abandoned3}(x)\right) & x > x_A \\ \eta(x) & x \leq x_A \end{cases} \quad \text{(S8)}$$

where x is distance downstream, x_A is the avulsion location, η_{new} is the new riverbed profile after avulsion, η is the riverbed profile before avulsion, and $\eta_{abandoned1}, \eta_{abandoned2}$, and $\eta_{abandoned3}$ are the three abandoned-lobe long profiles. The MIN operator here selects the abandoned profile that has the minimum mean elevation, $\bar{\eta}$, downstream of the avulsion node,

$$\bar{\eta} = \frac{1}{x_m - x_A} \int_{x_A}^{x_m} \eta(x)\, dx \qquad \text{(S9)}$$

where x_m is the downstream coordinate of the river mouth. For example, if $\eta_{abandoned2}(x)$ yielded a lower value of $\bar{\eta}$ than both $\eta_{abandoned1}(x)$ and $\eta_{abandoned3}(x)$ yield, then $\eta_{abandoned2}(x)$ was selected as the path downstream of the avulsion location. This procedure mimics the tendency of rivers to select steeper paths, fill in topographic lows (10, 23), and to reoccupy previously abandoned channels (24). After establishing the new flow path, lobe construction (Eqs. $\mathrm{S1}-\mathrm{S5}$) and avulsion setup (Eqs. $\mathrm{S6}$ and $\mathrm{S7}$) began anew.

To enable applicability across a wide range of river conditions, the model was normalized using the channel dimensions and the characteristic aggradation rate of the backwater zone, $\hat{v}_a = \frac{1}{(1-\lambda_p)} \frac{Q_s}{B_c L_b}$. Normalizing Eqs. ($\mathrm{S1}-\mathrm{S9}$) yields

$$\frac{\partial \eta^*}{\partial t^*} + \sigma^* = -\frac{1}{B^* \bar{q}^*{}_t} \frac{\partial q_t^*}{\partial x^*} \qquad \text{(S10)}$$

$$x_m^* = x^*|_{\eta_f^*(x^*) = \xi_o^*} \quad \text{(S11)}$$

$$\eta_f^*(x^*) = \eta^*(x^*) + 1 \qquad \text{(S12)}$$

$$\frac{\partial H_w^*}{\partial x^*} = \frac{S^* - S_f^*}{1 - Fr^2} + \frac{Fr^2}{1 - Fr^2}\frac{H^*}{B_w^*}\frac{dB_w^*}{dx^*} \qquad \text{(S13)}$$

$$C_f q_t^* = \alpha(\tau^*)^n \qquad \text{(S14)}$$

$$\Delta\eta^* \geq H^* \qquad \text{(S15)}$$

$$\Delta\eta^*(x^*) = \begin{cases} \eta_f^*(x^*) - \eta_{f,abandoned}^*(x^*) & \text{for } x^* \leq x_{m,abandoned}^* \\ \eta_f^*(x^*) - \xi_{sea}^* & \text{for } x^* > x_{m,abandoned}^* \end{cases} \qquad \text{(S16)}$$

$$\eta_{new}^*(x^*) = \begin{cases} \mathrm{MIN}\left(\eta_{abandoned1}^*(x^*), \eta_{abandoned2}^*(x^*), \eta_{abandoned3}^*(x^*)\right) & x^* > x_A^* \\ \eta^*(x^*) & x^* \leq x_A^* \end{cases} \qquad \text{(S17)}$$

$$\bar{\eta}^* = \frac{1}{x_m^* - x_A^*}\int_{x_A^*}^{x_m^*} \eta^*(x^*)\, dx^* \qquad \text{(S18)}$$

where $x^* = x/L_b$ is normalized distance downstream, $t^* = \frac{1}{(1-\lambda_p)}\frac{t}{H_c B_c L_b/Q_s}$ is normalized time and Q_s is volumetric sediment supply averaged over many flood cycles, $B^* = B/B_c$ is normalized lobe width, $H_w^* = H_w/H_c$ is the normalized depth of flow, $B_w^* = B_w/B_c$ is normalized width of flow, $S^* = S/(H_c/L_b)$ is the normalized bed slope, $S_f^* = Fr^2 C_f/(H_c/L_b)$ is the normalized friction slope, q_t^* is the Einstein number representing dimensionless bed-material transport (25, 26) and $\bar{q}^*{}_t$ is the time-averaged Einstein number. All elevation variables were normalized by the channel depth (e.g., $\xi_{sea}^* = \xi_{sea}/H_c$, $\eta^* = \eta/H_c$).

B. Model implementation

For comparison of results among the numerical backwater-scaled-avulsion model (Eqs. S1-S9), the analytical backwater-scaled-avulsion model (Eq. 4), the radially averaged model (Eq. 2), and the channel-averaged model (Eq. 3), we varied the normalized relative sea-level rise rates σ^* for constant values for the other input parameters that were representative of lowland deltas (Table S2). Parameter values correspond to the case of a delta that builds into a basin that is twice as deep as the channel ($H_b = 2H_c$) and experiences avulsions when the active lobe has aggraded to a height of half the channel depth ($H^* = \frac{H}{H_c} = 0.5$) above neighboring lobes. For all model runs we assumed deltas were composed of four lobes ($N = 4$) with a width of forty times the channel width ($B = 40B_c$) and 40% porosity ($\lambda_p = 0.4$), which are reasonable estimates for natural deltas (4, 21, 22, 27). Analytical models also required specification of lobe length, here set to the backwater length-scale ($L_A = L_b$). In contrast, the numerical backwater-scaled-avulsion model did not require specification of lobe length, as the model naturally produced lobe lengths between half and twice the backwater length-scale ($L_A = 0.5L_b$-$2L_b$) based on the location of maximum aggradation (Eq. S6).

The numerical model for backwater-scaled avulsions (Eqs. S1-S9) required six additional input parameters describing river flow, sediment transport, channel morphology, and a variable discharge regime, which is necessary to produce backwater-scaled avulsion nodes (1). These parameters are: bankfull Froude number in the normal-flow reach ($Fr_{n,bf}$), bankfull Shields number in the normal-flow reach ($\tau^*_{n,bf}$), friction factor (C_f), bankfull exceedance probability (F_{bf}), coefficient of variation of flow depth (CV), and a normalized flood duration (T_e^*). The bankfull exceedance probability F_{bf} describes the frequency of overbank floods, and the coefficient of variation CV describes the magnitude of large floods relative to low flows; together, F_{bf} and CV define a log-normal distribution of normal-flow depths (1, 28, 29). The distribution was discretized into twenty logarithmically spaced bins, with each bin i being described by normal-flow depth $H_{n,i}$ and probability F_i. We sampled the distribution at timescale set by the normalized flood duration $T_e^* = \frac{T_e}{L_b H_c B(1-\lambda_p)/Q_s}$, where T_e is the dimensional flood duration. For each flow bin i, we varied sediment supply ($Q_{s,i}$) using Engelund & Hansen (8) such that the normal-flow transport slope (S_{eq}) remained unchanged,

$$Q_{s,i} = B_c\sqrt{RgD^3}\,\frac{\alpha}{C_f}\left(\frac{H_n S_{eq}}{RD}\right)^n = B_c\sqrt{RgD^3}\,\frac{\alpha}{C_f}\left(\tau^*_{n,bf}H^*_{n,i}\right)^n$$

where $H^*_{n,i}$ is normal-flow depth of discharge bin i normalized by the channel depth ($H^*_{n,i} = H_{n,i}/H_c$) and $\tau^*_{n,bf} = \frac{H_c S_{eq}}{RD}$. Averaged over many flood cycles, the sediment supply Q_s is given by the linear combination of sediment supplies and occurrence probabilities for each flow bin,

$$Q_s = \sum_{i=1}^{20} Q_{s,i}F_i$$

Similar to other model parameters, the parameters exclusive to the numerical model were held constant at values representative of lowland deltas ($Fr_{n,bf} = 0.17$, $\tau^*_{n,bf} = 1$, $C_f = 0.005$, $F_{bf} = 0.05$, $CV = 0.53$, $T^*_e = 0.001$; Table S2).

The numerical model (Eqs. S1-S9) also required specification of initial conditions. At the start of each model run, the initial topography of each delta lobe was assumed planar with a uniform downstream slope set to the transport slope for normal flow, similar to previous studies (3, 17, 30). Following previous work, each model run began with a spin-up phase during which the river occupied each lobe at least once, and thus the effect of initial conditions was minimized (1).

Following the model spin-up, the numerical model (Eqs. S1-S9) was run for 13 avulsion cycles. We computed the average time T_A between avulsions and calculated avulsion frequency using $f_A \equiv 1/T_A$. Cycles 4, 7, 10, and 13 were excluded from the average because these cycles featured significant trunk-channel sedimentation, which was not observed during most avulsion cycles and violated simplifying assumptions in the analytical model. As documented previously (1), trunk-channel sedimentation in the numerical model occurs every $N - 1$ avulsions, and is associated with downstream translation of the avulsion node in tandem with shoreline progradation, similar to that observed on the Yellow River delta (15).

In addition to comparison among models, we also tested the analytical backwater-scaled-avulsion model (Eq. 4), the radially averaged model (Eq. 2), and the channel-averaged model (Eq. 3) directly against field data pertaining to the Holocene period for 6 natural deltas where all model parameters could be constrained (Fig. 2, Fig. S1). For each natural delta, we calculated how f_A varied with relative sea-level rise in the range $\sigma^* =$ -$1 - 10$, holding all other parameters to constant values specific to each delta (Table S2). Using the minimum and maximum f_A among field sites for a given σ^* value, we defined an envelope of analytical model predictions that could be compared to all field data (Fig. 2, Fig. S1)

C. Nomenclature

Symbol	Meaning	Dimensions ($L = \text{length}$, $M = \text{mass}$, $T = \text{time}$, $1 = \text{dimensionless}$)
A_Δ	Delta land area	L^2
B	Lobe width	L
B_c	Channel width	L
B^*	Lobe width normalized by channel width	1
D	Lobe-progradation distance	L
D^*	Lobe-progradation distance normalized by backwater length-scale	1
f_A	Avulsion frequency	T^{-1}
f_A^*	Avulsion frequency normalized by maximum possible avulsion frequency	1
H	Aggradation thickness necessary for avulsion	L
H^*	Avulsion threshold	1
H_b	Offshore basin depth	L
H_b^*	Offshore basin depth normalized by channel depth	1
H_c	Channel depth	L
L_A	Lobe length (or avulsion length)	L
L_A^*	Normalized lobe length	1
L_b	Backwater length-scale	L
n	Number of avulsions before a given lobe is reoccupied	1
N	Number of delta lobes	
Q_s	Volumetric sediment supply averaged over many flood cycles	L^3T^{-1}
S	Channel-bed slope	1
T_A	Time between avulsions	T
v_a	Aggradation rate	LT^{-1}
v_a^*	Aggradation rate normalized by characteristic aggradation rate of the backwater zone.	
$\hat{v}_a$	Characteristic aggradation rate of the backwater zone	LT^{-1}
σ	Relative sea-level rise rate	LT^{-1}
σ^*	Relative sea-level rise rate normalized by sediment supplied to the whole delta	1

D. Derivation of analytical model for backwater-scaled avulsions

Our backwater-scaled analytical model averages mass balance over an avulsion cycle where lobes are assumed to build at a fixed length L_A set by backwater hydrodynamics (3, 31, 32), and the river aggrades to thickness H before an avulsion occurs (2, 14, 15). The trunk channel upstream of the avulsion node aggrades during construction of the first lobe (Fig. 1C), such that aggradation occurs only downstream of the avulsion node for subsequent avulsion cycles. We assume a uniform riverbed slope, S, and a vertical delta foreset. These assumptions are relaxed in the full numerical model, but here allow for an analytical approximation:

$$\frac{Q_s T_A}{\left(1-\lambda_p\right)} = \begin{cases} (L_A - D)BH + DB(H_b + z + DS/2) & \text{if } D \geq 0 \\ L_A BH & \text{if } D < 0 \end{cases} \quad (S19)$$

where D is lobe-progradation distance just prior to avulsion, and z is the magnitude of sea-level rise over an avulsion cycle. For $D \geq 0$, the first two terms on the right-hand side account for deposition on the delta topset and progradation of the foreset (Fig. 1B-C). For $D < 0$, sedimentation is only on the topset. Combining Eq. ($S19$) and $f_A \equiv 1/T_A$ and rearranging for f_A results in the solution given by Eq. (4).

Geometric constraints (15) dictate that shoreline progradation is:

$$D = L_b \left(H^* - \frac{z}{H_c}\right) \quad (S20)$$

and that the magnitude of sea-level rise during an avulsion cycle is

$$z = n\sigma T_A \quad (S21)$$

where n is the number of avulsions that occur before lobe reoccupation, which —for random switching amongst topographic low areas— is

$$n = \frac{N+1}{2} \quad (S22)$$

where N is the total number of lobes (2).

Some parameter combinations can violate model assumptions, and so we impose three constraints. Marine transgression between avulsions must not drown the avulsion node,

$$D > -L_A \quad (S23)$$

and lobes must not prograde greater than an avulsion length between avulsions,

$$D < L_A \quad (S24)$$

If Eqs. ($S23$) or ($S24$) are unsatisfied, then the avulsion node is forced to migrate upstream or downstream respectively, and the backwater-scaled analytical model is not applicable, but the numerical model still holds. Lastly, sea-level fall cannot drop below the basin floor,

$$z > -H_b \quad (S25)$$

or else the channel is predicted to incise and avulsions do not occur.

Similar to the numerical model, the analytical model was normalized using the channel dimensions and characteristic aggradation rate of the backwater zone, $\hat{v}_a = \frac{Q_s}{B_c L_b}$. Normalizing Eqs. ($S19-25$) yields

$$\frac{1}{f_A^*} = \begin{cases} (L_A^* - D^*)B^*H^* + D^*B^*\left(H_b^* + z^* + \frac{1}{2}D^*\right) & \text{if } D \geq 0 \\ L_A^*B^*H^* & \text{if } D < 0 \end{cases} \quad (S26)$$

$$D^* = H^* - z^* \quad (S27)$$

$$z^* = \sigma^* T_A^* / B^* \quad (S28)$$

$$n = \frac{N+1}{2} \quad (S29)$$

$$D^* > -L_A^* \quad (S30)$$

$$D^* < L_A^* \quad (S31)$$

where $f_A^* = \frac{f_A}{Q_s/H_c B_c L_b (1-\lambda_p)}$ is normalized avulsion frequency, $D^* = D/L_b$ is normalized shoreline-progradation distance, $L_A^* = L_A/L_b$ is normalized lobe length (or avulsion length), and $z^* = z/H_c$ is normalized magnitude of relative sea-level rise between avulsions on a given lobe. Rearranging Eq. ($S26$) results in a normalized version of Eq. (4),

$$f_A^* = \begin{cases} \dfrac{1}{(L_A^* - D^*)H^*B^* + D^*B^*\left(H_b^* + z^* + \frac{1}{2}D^*\right)} & \text{if } D^* \geq 0 \\ \dfrac{1}{L_A^*H^*B^*} & \text{if } D^* < 0 \end{cases} \quad (S32)$$

The analytical model, Eqs. (4) and (S32), is a general solution that encompasses the channel-averaged model (Eq. 3), which can be recovered by assuming no shoreline progradation ($D = D^* = 0$) and no floodplain ($B^* = B/B_c = 1$), and the radially averaged model (Eq. 2), with a further assumption that the delta area reflects an equilibrium between sediment supply and sea level rise ($nL_A B = \Delta A = \frac{1}{(1-\lambda_p)}\frac{Q_s}{\sigma}$, or equivalently $\sigma^* = L_A^* = 1$). The normalized form of the radially averaged model (Eq. 2) is

$$f_A^* = \frac{\sigma^*}{nB^*H^*} \quad (S33)$$

Similarly, the normalized channel-averaged sediment mass balance model (Eq. 3) is

$$f_A^* = \frac{1}{L_A^* H^*} \quad (S34)$$

Incorporating a lobe width into the channel-averaged model ($B_c \rightarrow B$ in Eq. 3) yields

$$f_A^* = \frac{1}{L_A^* H^* B^*} \quad (S35)$$

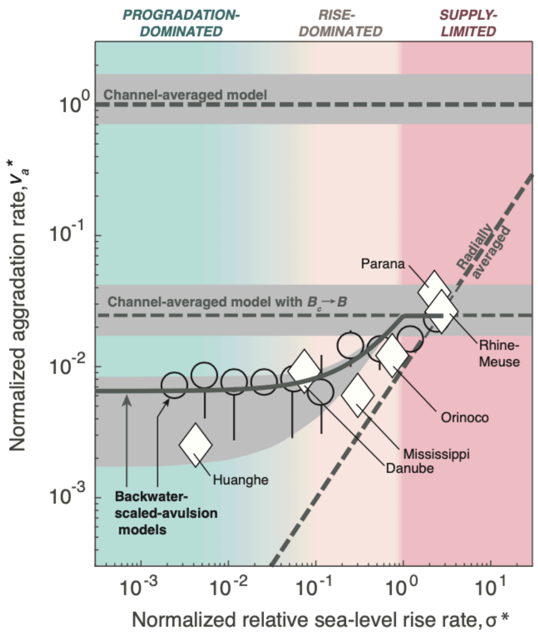

Fig. S1. Model results for normalized aggradation rate $v_a^* = \frac{v_a}{Q_s/(1-\lambda_p)H_cB_cL_b}$ as a function of normalized relative sea-level rise σ^*, showing progradation-dominated, rise-dominated, and supply-limited regimes. Aggradation rates reported in Table S1. Black circles and error bars show the median, minimum, and maximum from 13 avulsions that occurred for each numerical backwater-scaled-avulsion model run. Gray solid line is analytical backwater-scaled-avulsion model (Eq. 4; Eq. S32), and dashed lines are radially averaged model (Eq. 2; Eq. S33), channel-averaged model (Eq. 3; Eq. S34), and channel-averaged model incorporating a lobe width (Eq. 3 with $B_c \rightarrow B$; Eq. S35) for $H^* = 0.5, L_A = L_b, H_b = 2H_c, N = 4,$ and $B = 40B_c$. White diamonds are data for cases where all parameters are constrained including pre-industrial historical avulsions on the Huanghe, and avulsions during the Holocene period for the other deltas. Gray shaded regions are envelopes of analytical model solutions using H^*, L_A, and H_b values reported for each natural delta (Table S2).

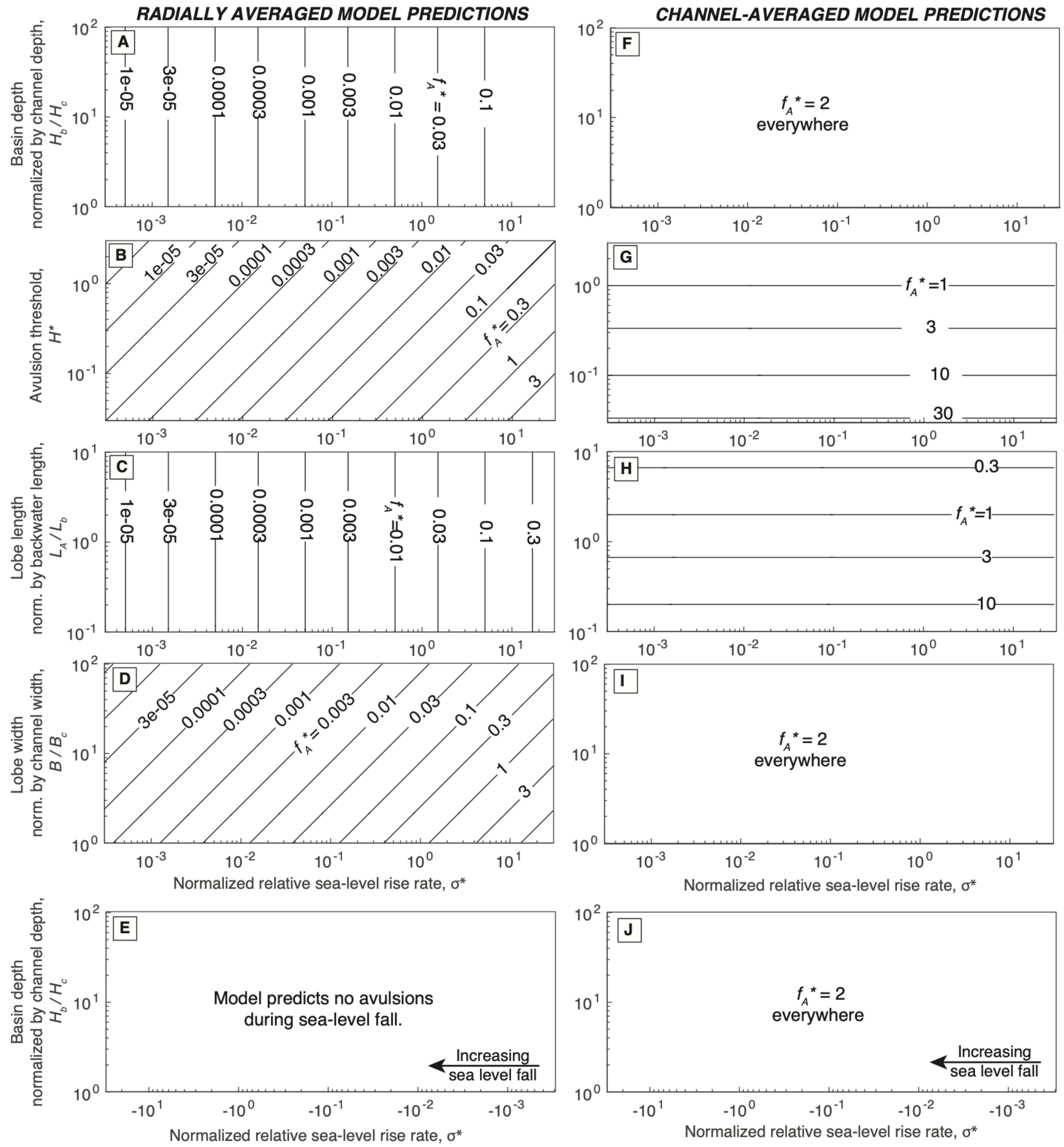

Fig. S2. Normalized avulsion frequency predictions according to the radially averaged model (A-E) and channel-averaged model (F-J), with systematic variation of basin depth, avulsion threshold, lobe length, and lobe width. Other model parameters were set to constant values typical of large lowland deltas ($H^* = 0.5, L_A = L_b, H_b = 2H_c$, and $B = 40B_c$; Table S2). Predictions for falling sea level and basin depth are shown in panels E and J. Analytical backwater-scaled-avulsion model predictions for the same parameter space are shown in Figure 3.

Table S1. Field data used in this study

River	H_c [m]	B_c [m]	L_b [km]	Q_s [km^3/year]	H_b [m]	L_A [km]	σ_{eu} [mm/yr]	σ_{sub} [mm/yr]	σ [mm/yr]	B [km]	N [-]	λ_p [-]	v_a [mm/yr]	T_A [yr]	f_A [1/kyr]
Parana	11.8	1270	295.0	3.0E-02	40	210	1.6	1.4	3.0	50.8	4	0.4	5	1633	0.6
Danube	6.3	1250	125.0	2.5E-02	50	95	–	–	0.2	50	4	0.4	2.5	1991	0.5
Nile	16.2	240	254.0	4.5E-02	120	210	1.5	3	4.5	9.6	4	0.4	–	–	–
Mississippi	21.0	650	480.0	1.5E-01	80	490	1.3	1	2.3	26	4	0.4	10	1250	0.8
Assiniboine	4.2	100	8.4	3.6E-04	7	12	–	–	–	4	4	0.4	1.4	1000	1.0
Rhine-Meuse	5.0	700	45.5	1.2E-03	18	51	1.5	0.1	1.6	28	4	0.4	1.6	1450	0.7
Magdalena	6.0	1100	63.2	8.3E-02	200	67	1.5	1.4	2.9	44	4	0.4	3.8	–	–
Orinoco	8.0	2000	133.3	5.7E-02	110	78	1.3	1.4	2.7	80	4	0.4	2.1	1000	1.0
Mid-Amazon	12.0	3000	400.0	4.5E-01	50	404	1.5	1.4	2.9	120	4	0.4	5	–	–
Upper Rhone	5.4	377	135.2	1.2E-02	70	–	1.5	1.4	2.9	15.08	4	0.4	2	1450	0.7
Huanghe	3.5	500	35.0	4.2E-01	30	31	0.3	1.4	1.7	20	4	0.4	100	7	142.9
Brahmaputra	7.0	3300	70.0	2.0E-01	80	–	1.4	10	11.4	132	4	0.4	20	500	2.0
Goose	2.0	100	0.9	1.3E-04	10	–	–	–	-3	4	4	0.4	1.98	333	3.0
Mitchell	7.0	100	23.3	1.1E-03	15	–	–	–	-0.25	4	4	0.4	–	63	16.0
Trinity	5.0	200	31.3	2.3E-03	8	–	–	–	4.2	8	4	0.4	1.1	–	–

Bankfull channel depth (H_c), channel width (B_c), aggradation rates (v_a), and avulsion frequencies (f_A) are reported in (33), and avulsion lengths (L_A) and backwater lengths (L_b) are reported in (3, 15). Avulsions occurred during the Holocene period, with the exception of the Huanghe where pre-industrial historical avulsions are documented (15). Basin depths (H_b) are reported in (34). Sediment supplies (Q_s) are reported in (35), and were converted here to volumetric rates using a sediment density of $2650\ \mathrm{kg/m^3}$. The avulsion threshold for each site was estimated using $H^* = v_a/(f_A H_c)$ following (15). Eustatic sea-level rise (σ_{eu}) was estimated from (36) using the average rate during the period that avulsion frequency was measured. Coastal subsidence rates (σ_{sub}) are reported in (37–41), and for sites where data were unavailable we assumed an average value for deltas (1.4 mm/yr) following (42). Relative sea-level rise (σ) was calculated as the sum of eustatic sea level rise and coastal subsidence ($\sigma = \sigma_{eu} + \sigma_{subs}$). Data for the Danube, Goose, Mitchell, and Trinity were compiled from recent studies (30, 43–45). Deltas were assumed to be composed of four lobes ($N = 4$) with width of forty times the channel width ($B = 40B_c$) and 40% porosity ($\lambda_p = 0.4$), which are reasonable estimates for natural deltas (4, 21, 22, 27). Empty table entries indicate data were not available.

Table S2. Normalized model input parameters

River or model run	σ^* [-]	$\frac{H_b}{H_c}$ [-]	H^* [-]	$\frac{L_A}{L_b}$ [-]	$\frac{B}{B_c}$ [-]	N [-]	$Fr_{n,bf}$ [-]	$\tau^*_{n,bf}$ [-]	C_f [-]	F_{bf} [-]	CV [-]	T^*_e [-]
Parana	2.3	3.4	0.69	0.7	40	4	0.09	0.98	0.005	0.12	0.18	1.9E-04
Danube	0.076	7.9	0.79	0.8	40	4	0.10	0.66	0.005	0.10	0.27	3.0E-03
Nile	3.7	7.4	–	0.8	40	4	0.11	1.62	0.005	0.05	0.65	6.4E-02
Mississippi	0.29	3.8	0.60	1.0	40	4	0.09	1.88	0.005	0.06	0.44	1.8E-03
Assiniboine	–	1.7	0.33	1.4	40	4	0.32	2.63	0.005	–	–	2.8E-03
Rhine-Meuse	2.6	3.6	0.46	1.1	40	4	0.15	0.69	0.005	–	–	2.0E-04
Magdalena	0.15	33.3	–	1.1	40	4	0.14	1.02	0.005	–	–	5.5E-03
Orinoco	0.77	13.8	0.26	0.6	40	4	0.11	1.00	0.005	0.43	0.61	7.4E-04
Mid-Amazon	0.47	4.2	–	1.0	40	4	0.08	0.90	0.005	–	–	8.7E-04
Upper Rhone	1.0	12.9	0.54	–	40	4	0.09	0.61	0.005	–	–	6.4E-04
Huanghe	0.0043	8.6	0.20	0.9	40	4	0.14	2.19	0.005	0.22	0.91	3.8E-01
Brahmaputra	0.80	11.4	1.43	–	40	4	0.14	0.88	0.005	0.08	0.68	3.7E-03
Goose	-0.13	5.0	0.33	–	40	4	0.68	8.46	0.005	–	–	2.0E-02
Mitchell	-0.033	2.1	–	–	40	4	0.24	–	0.005	–	–	1.9E-03
Trinity	0.69	1.6	–	–	40	4	0.18	2.00	0.005	–	–	2.1E-03
Backwater-scaled numerical model	-1 – 10	3	0.5	–	40	4	0.17	1.00	0.005	0.05	0.53	1.0E-03
Analytical models (radially averaged, channel-averaged, backwater-scaled)	-1 – 10	3	0.5	1	40	4	–	–	–	–	–	–
Envelope of analytical model solutions in Fig. 2 & Fig. S1	-1 – 10	3 – 14	0.2 – 0.7	0.5 – 2	40	4	–	–	–	–	–	–

All values were calculated using field data in Table 1 and discharge time series in Ganti et al. (15). $\sigma^* = \frac{\sigma}{Q_s/nBL_b(1-\lambda_p)}$ is normalized relative sea-level rise rate, H_b/H_c is basin depth normalized by channel depth, H^* is avulsion threshold, L_A/L_b is avulsion length normalized by backwater length-scale, B/B_c is lobe width normalized by channel width, $Fr_{n,bf}$ is bankfull Froude number in the normal flow reach, $\tau^*_{n,bf}$ is bankfull Shields number in the normal flow reach, C_f is friction coefficient, F_{bf} is bankfull exceedance probability, CV is coefficient of variation of stage height, and $T^*_e = \frac{T_e}{H_c B_c L_b(1-\lambda_p)/Q_s}$ is normalized flood duration where $T_e = 1$ month. Empty table entries indicate data were not available.

Table S3. Modern relative sea-level rise rates and expected avulsion frequencies from the backwater-scaled-avulsion model

River	σ [mm/yr]	σ^* [-]	T_A [yr]	f_A [1/kyr]
Parana	2–3	1.5–2.3	1797	0.6
Danube	1.2	0.46	1423	0.7
Nile	4.8	0.40	–	–
Mississippi	5–25	0.64–3.2	897	1.1
Assiniboine	–	–	–	–
Rhine-Meuse	–	–	–	–
Magdalena	5.3–6.6	0.27–0.34	–	–
Orinoco	0.8–3	0.23–0.87	269–833	1.2–3.7
Mid-Amazon	–	–	–	–
Upper Rhone	2–6	0.73–2.2	–	–
Huanghe	8–23	0.02–0.06	5–6	170–220
Brahmaputra	8–18	0.56–1.3	–	–
Goose	–	–	–	–
Mitchell	–	–	–	–
Trinity	–	–	–	–

Modern relative sea-level rise rates ($\sigma = \sigma_{eu} + \sigma_{sub}$, where σ_{eu} and σ_{sub} are eustatic sea-level rise and land subsidence components, respectively) were measured by tide gauges on each delta over the twentieth century, as reported by Syvitski et al. (2009). Corresponding normalized relative sea-level rise (σ^*) was calculated assuming no change in other model parameters (Table S1). Modern expectations for avulsion timescale (T_A) and avulsion frequency ($f_A \equiv 1/T_A$) were determined using the analytical backwater-scaled-avulsion model. Empty table entries indicate data were not available.

References for Supplementary Information

1. A. J. Chadwick, M. P. Lamb, A. J. Moodie, G. Parker, J. A. Nittrouer, Origin of a preferential avulsion node on lowland river deltas. *Geophys. Res. Lett.* **46**, 4267–4277 (2019).
2. V. Ganti, M. P. Lamb, A. J. Chadwick, Autogenic erosional surfaces in fluvio-deltaic stratigraphy from floods, avulsions, and backwater hydrodynamics. *J. Sediment. Res.* (2019).
3. P. Chatanantavet, M. P. Lamb, J. A. Nittrouer, Backwater controls of avulsion location on deltas. *Geophys. Res. Lett.* **39** (2012).
4. G. Parker, T. Muto, Y. Akamatsu, W. E. Dietrich, J. W. Lauer, Unravelling the conundrum of river response to rising sea-level from laboratory to field. Part II. The Fly-Strickland River system, Papua New Guinea. *Sedimentology* **55**, 1657–1686 (2008).
5. J. B. Swenson, V. R. Voller, C. Paola, G. Parker, J. G. Marr, Fluvio-deltaic sedimentation: A generalized Stefan problem. *Eur. J. Appl. Math.* **11**, 433–452 (2000).
6. S. Kostic, G. Parker, Progradational sand-mud deltas in lakes and reservoirs. Part 1. Theory and numerical modeling. *J. Hydraul. Res.* **41**, 127–140 (2003).
7. M. P. Lamb, J. A. Nittrouer, D. Mohrig, J. Shaw, Backwater and river plume controls on scour upstream of river mouths: Implications for fluvio-deltaic morphodynamics. *J. Geophys. Res.* **117**, F01002 (2012).
8. F. Engelund, E. Hansen, A monograph on sediment transport in alluvial streams. *Tech. Univ. Denmark 0stervoldgade 10, Copenhagen K.* (1967).
9. J. B. Swenson, V. R. Voller, C. Paola, G. Parker, J. G. Marr, Fluvio-deltaic sedimentation: A generalized Stefan problem. *Eur. J. Appl. Math.* **11**, 433–452 (2000).
10. R. Slingerland, N. D. Smith, River Avulsions and Their Deposits. *Annu. Rev. Earth Planet. Sci.* **32**, 257–285 (2004).
11. E. A. Hajek, D. A. Edmonds, Is river avulsion style controlled by floodplain morphodynamics? *Geology* **42**, 199–202 (2014).
12. C. Paola, Quantitative models of sedimentary basin filling. *Sedimentology* **47**, 121–178 (2000).
13. W. E. Galloway, Process framework for describing the morphologic and stratigraphic evolution of

deltaic depositional systems (1975).

14. D. Mohrig, P. L. Heller, W. J. Lyons, Interpreting avulsion process from ancient alluvial sequences : Guadalope-Matarranya system (northern Spain) and Wasatch Formation (western Colorado). 1787–1803 (2000).

15. V. Ganti, Z. Chu, M. P. Lamb, J. A. Nittrouer, G. Parker, Testing morphodynamic controls on the location and frequency of river avulsions on fans versus deltas: Huanghe (Yellow River), China. *Geophys. Res. Lett.* **41**, 7882–7890 (2014).

16. V. Ganti, A. J. Chadwick, H. J. Hassenruck-Gudipati, M. P. Lamb, Avulsion cycles and their stratigraphic signature on an experimental backwater-controlled delta. *J. Geophys. Res. Earth Surf.* **121**, 1651–1675 (2016).

17. K. M. Ratliff, E. H. W. Hutton, A. B. Murray, Exploring Wave and Sea-Level Rise Effects on Delta Morphodynamics With a Coupled River-Ocean Model. *J. Geophys. Res. Earth Surf.* **123**, 2887–2900 (2018).

18. A. P. Nicholas, R. E. Aalto, G. H. S. Smith, A. C. Schwendel, Hydrodynamic controls on alluvial ridge construction and avulsion likelihood in meandering river floodplains. *Geology* **46**, 639–642 (2018).

19. D. J. Jerolmack, C. Paola, Complexity in a cellular model of river avulsion. *Geomorphology* **91**, 259–270 (2007).

20. E. A. Hajek, M. A. Wolinsky, Simplified process modeling of river avulsion and alluvial architecture: Connecting models and field data. *Sediment. Geol.* **257**–**260**, 1–30 (2012).

21. J. Pang, S. Si, The Estuary Changes of Huanghe River I. Changes in modern time. *Oceanol. Limnol. Sin.* **2** (1979).

22. J. M. Coleman, H. H. Roberts, G. W. Stone, Mississippi River delta: an overview. *J. Coast. Res.* **14** (1998).

23. K. M. Straub, C. Paola, D. Mohrig, M. A. Wolinsky, T. George, Compensational Stacking of Channelized Sedimentary Deposits. *J. Sediment. Res.* **79**, 673–688 (2009).

24. M. D. Reitz, D. J. Jerolmack, Experimental alluvial fan evolution: Channel dynamics, slope controls, and shoreline growth. *J. Geophys. Res.* **117**, F02021 (2012).

25. H. A. Einstein, “The bed-load function for sediment transportation” in *Open Channel Flow Technical Bulletin*, (U.S. Department of Agriculture, Washington, D.C, 1950), p. 1026.

26. G. Parker, Hydraulic geometry of active gravel rivers in *ASCE J Hydraul Div*, (1979), pp. 1185–1201.

27. A. T. Hayden, *et al.*, Formation of sinuous ridges by inversion of river-channel belts in Utah, USA, with implications for Mars. *Icarus* **332**, 92–110 (2019).

28. D. W. LeBoutillier, P. R. Waylen, A stochastic model of flow duration curves. *Water Resour. Res.* **29**, 3535–3541 (1993).

29. J. R. Stedinger, Frequency analysis of extreme events. *Handb. Hydrol.* (1993).

30. K. E. Moran, J. A. Nittrouer, M. M. Perillo, J. Lorenzo-Trueba, J. B. Anderson, Morphodynamic modeling of fluvial channel fill and avulsion time scales during early Holocene transgression, as substantiated by the incised valley stratigraphy of the Trinity River, Texas. *J. Geophys. Res. Earth Surf.* **122**, 215–234 (2017).

31. V. Ganti, A. J. Chadwick, H. J. Hassenruck-Gudipati, B. M. Fuller, M. P. Lamb, Experimental river delta size set by multiple floods and backwater hydrodynamics. *Sci. Adv.* **2**, e1501768 (2016).

32. D. J. Jerolmack, J. B. Swenson, Scaling relationships and evolution of distributary networks on wave-influenced deltas. *Geophys. Res. Lett.* **34** (2007).

33. D. J. Jerolmack, D. Mohrig, Conditions for branching in depositional rivers. *Geology* **35**, 463 (2007).

34. J. P. M. Syvitski, Y. Saito, Morphodynamics of deltas under the influence of humans. *Glob. Planet. Change* **57**, 261–282 (2007).

35. J. D. Milliman, J. P. M. Syvitski, Geomorphic/Tectonic Control of Sediment Discharge to the Ocean: The Importance of Small Mountainous Rivers. *J. Geol.* **100**, 525–544 (1992).

36. R. Bintanja, R. S. W. van de Wal, J. Oerlemans, Modelled atmospheric temperatures and global sea levels over the past million years. *Nature* **437**, 125 (2005).

37. S. Jelgersma, “Land subsidence in coastal lowlands” in *Sea-Level Rise and Coastal Subsidence*, (Springer, 1996), pp. 47–62.

38. T. E. Törnqvist, *et al.*, Mississippi Delta subsidence primarily caused by compaction of Holocene

strata. *Nat. Geosci.* **1**, 173 (2008).

39. S.-Y. Yu, T. E. Törnqvist, P. Hu, Quantifying Holocene lithospheric subsidence rates underneath the Mississippi Delta. *Earth Planet. Sci. Lett.* **331**, 21–30 (2012).
40. J. P. M. Syvitski, Deltas at risk. *Sustain. Sci.* **3**, 23–32 (2008).
41. J. D. Milliman, J. M. Broadus, F. Gable, Environmental and economic implications of rising sea level and subsiding deltas: the Nile and Bengal examples. *Ambio*, 340–345 (1989).
42. J. P. Ericson, C. J. Vörösmarty, S. L. Dingman, L. G. Ward, M. Meybeck, Effective sea-level rise and deltas: causes of change and human dimension implications. *Glob. Planet. Change* **50**, 63–82 (2006).
43. A. G. Nijhuis, *et al.*, Fluvio-deltaic avulsions during relative sea-level fall. *Geology* **43**, 719–722 (2015).
44. T. I. Lane, R. A. Nanson, B. K. Vakarelov, R. B. Ainsworth, S. E. Dashtgard, Evolution and architectural styles of a forced-regressive Holocene delta and megafan, Mitchell River, Gulf of Carpentaria, Australia. *Geol. Soc. London, Spec. Publ.* **444**, 305–334 (2017).
45. L. Giosan, *et al.*, Young Danube delta documents stable Black Sea level since the middle Holocene: Morphodynamic, paleogeographic, and archaeological implications. *Geology* **34**, 757–760 (2006).